Applied Catalysis B: Environmental 258 (2019) 117793

Contents lists available at ScienceDirect

Applied Catalysis B: Environmental

journal homepage: www.elsevier.com/locate/apcatb

A flexible Cu-based catalyst system for the transformation of fructose to furanyl ethers as potential bio-fuels

Junnan Wei[a], Ting Wang[a], Xuejuan Cao[a], Huai Liu[a], Xing Tang[a,b,*], Yong Sun[a,b], Xianhai Zeng[a,b], Tingzhou Lei[c], Shijie Liu[d], Lu Lin[a,b,*]

[a] Xiamen Key Laboratory of Clean and High-valued Applications of Biomass, College of Energy, Xiamen University, Xiamen 361102, China
[b] Fujian Engineering and Research Center of Clean and High-valued Technologies for Biomass, Xiamen University, Xiamen 361102, China
[c] Henan Key Lab of Biomass Energy, Henan 450008, China
[d] State University of New York, College of Environmental Science and Forestry,1 Forestry Drive, Syracuse, NY 13210, USA

ARTICLE INFO

Keywords:
CuO(5)-USY
fructose
5-alkoxymethylfurfurals and 2, 5-bis (alkoxymethyl)furans
dehydration
reductive etherification

ABSTRACT

Biomass-derived furanyl ethers, such as 5-alkoxymethylfurfurals (AMFs) and 2,5-bis(alkoxymethyl)furans (BAMFs), can be employed as promising biofuels or additives. The development of multifunctional catalysts for the efficient production of furanyl ethers from sugars through 5-hydroxymethylfurfural (HMF) as an intermediate is highly desirable but challenging, because multiple reactions including dehydration, etherification and hydrogenation get involved and the side reaction of sugars and HMF to form humins is inevitable. In this contribution, we found that the introduction of CuO resulted in the generation of Lewis acid sites at the cost of Bronsted acid sites over CuO-USY catalysts through the formation of Al-O-Cu(II) species. The dispersity of CuO particles and the amount of Lewis acid sites could be manipulated by adjusting the loading of CuO. If 5 wt% CuO was supported on USY zeolite to give a CuO(5)-USY catalyst, CuO particles with a high dispersity (36.4%) afforded abundant Lewis acid sites (457.1 μmol/g). Lewis acid over CuO(5)-USY greatly promoted the acid-catalyzed dehydration of fructose to HMF and HMF etherification to AMFs, resulting in a HMF yield up to 86.2% from fructose and AMFs yields greater than 90% from HMF. Interestingly, a combination of CuO(5)-USY and a small amount of metallic Cu powder was able to offer desirable BAMFs yields by the reductive etherification of HMF under hydrogen atmosphere. As a result, 5-methoxymethylfurfural (MMF) of 79.6% and 2,5-bis(methoxymethyl)furan (BMMF) yield of 74.5% were achieved from fructose through HMF as an intermediate in the presence of CuO(5)-USY alone or with metallic Cu as a co-catalyst. Therefore, the above Cu-based catalyst system holds the promise to flexibly produce a family of AMFs or BAMFs from fructose via a facile two-step approach.

1. Introduction

The ever-increasing environmental deterioration caused by the depletion of fossil resources drives powerful momentum to produce chemicals and clean fuels from renewable lignocellulosic biomass [1], One of the main components of lignocellulose is cellulose, a polysaccharide linked by a group of glucose molecules through glucosidic bonds. The main approaches for the utilization of cellulose initially involve the chemical and/or biological hydrolysis cellulose to glucose [2]. Glucose can be isomerized into fructose [3], from which one can readily envision a number of promising liquid fuel components such as γ-valerolactone [4,5], 2,5-dimethylfuran [6], ethyl levulinate [7], and furanyl ethers [8–13].

Furanyl ethers with different length of carbon chains have different energy density and miscibility with commercial fuels, thus it is of great interest to investigate the application and synthesis of furanyl ethers from biomass and its derivatives. One example is 5-ethoxymethylfurfural (EMF) that can be used directly as fuel or fuel additive due to its high energy density (30.3 MJ/L), approximately 30% higher than that of bioethanol (23.5 MJ/L) and close to that of diesel (33.6 MJ/L) or gasoline (31.1 MJ/L) [14]. Previous work in the production of EMF has operated by first forming 5-(chloromethyl)furfural from fructose in HCl solution, then nucleophilic substitution of CMF with ethanol formed EMF and HCl [14]. Although high EMF yield was obtained in this process, there are concerns about HCl recyclability and the introduction of unreacted halides into automobile fuel systems, which could cause

* Corresponding authors at: Xiamen Key Laboratory of Clean and High-valued Applications of Biomass, College of Energy, Xiamen University, Xiamen 361102, China.
E-mail addresses: x.tang@xmu.edu.cn (X. Tang), lulin@xmu.edu.cn (L. Lin).

https://doi.org/10.1016/j.apcatb.2019.117793
Received 3 April 2019; Received in revised form 16 May 2019; Accepted 29 May 2019
Available online 30 May 2019
0926-3373/

premature wear [14,15]. Another approach for producing EMF involves the formation of 5-hydroxymethylfurfural (HMF) as an intermediate via acid-catalyzed dehydration of fructose, then HMF reacted with ethanol to form EMF [10]. HMF also can be etherified with other C1-C4 alcohols to produce a variety of mono-ethers with superior properties as fuel alternative [16]. For instance, 5-(t-butoxymethyl)furfural derived from the etherification of HMF with t-butanol can be blended in commercial diesel at a blending rate up to 40%, resulting in substantial increase in the cetane number of the blended diesel fuel [17]. On the other hand, the etherification products of HMF with fatty alcohols have high molecular weights, which are suitable for being applied as cold-flow improvers to reduce the viscosity of biodiesel [9].

2, 5-Bis(alkoxymethyl)furans (BAMFs), furanyl di-ethers, are more ideal candidates to be employed as diesel additives because they have much better miscibility with commercial diesel than mono-ethers [18,19]. For instance, 2,5-bis(methoxymethyl)furan (BMMF) is completely miscible with commercial diesel [20]. The synthesis of BAMFs can be realized by coulping transfer hydrgenation and etherification of HMF in alcohols through Meerwein–Ponndorf–Verley (MPV) reduction [21]. Recently, Sn-based and Zr-based catalysts have successfully provided a high BAMFs yield through transfer hydrgenation and etherification of HMF in isopropanol or isobutanol [22–25]. However, these catalysts failed to offer high yields of BAMFs in n-alcohols (e.g. methanol, ethanol, n-propanol, etc.), because the higher reduction potential of primary alcohols makes the abstraction of hydrogen from primary alcohols for MPV reduction more difficult than that from secondary alcohols [26]. BAMFs also can be obtained from HMF by hydrogenation and etherification in alcohols using molecular hydrogen as H-donor. Balakrishnan et al. studied one-pot reductive etherification of HMF in ethanol, achieving a 2,5-bis(ethoxymethyl)furan (BEMF) yield of 64.0% over a combination of $PtSn/Al_2O_3$ and Amberlyst-15 [27]. Mu et al. proposed a two-step strategy to achieve 70% yield of BMMF from HMF in methanol by using a Cu/SiO_2 and HZSM-5 co-catalyst system [20]. It is highly desirable to produce BAMFs starting from sugars in the presence of a multifunctional catalyst from the perspective of economy. More recently, bi-functional Co-400 catalyst was developed by Li et al. for the formation of BMMF in methanol by hydrogenation and etherification of HMF, providing the highest BMMF yield up to 98.5% [28]. However, Co-400 failed to catalyze the dehydration of fructose owing to the absence of Bronsted acidity. Therefore, the development of efficient multifunctional catalysts or catalytic systems that are able to catalyze dehydration, hydrogenation and etherification is of crucial importance to the formation of BAMFs from sugars.

Copper-based catalysts are capable of catalyzing numerous reactions such as hydrogenation [29–33], hydrogenolysis [34–36], oxidation [37], etc. Many copper-based catalysts (e.g. Cu-ZnO, Cu-PMO, Cu/SiO_2, CuZn alloy) were reported to be effective for the hydrogenation of aldehyde group in HMF [38], but no work previously demonstrated that copper-based catalysts are capable of catalyzing the dehydration of sugars or the etherification of HMF. In this work, highly dispersed copper oxide over ultra-stable Y zeolite (CuO(5)-USY) was found to bring about an abundance of acid sites, which greatly contribute to develop a facile two-step approach for the production of 5-methoxymethylfurfural (MMF) from fructose over CuO(5)-USY by the acid-catalyzed dehydration of fructose followed by the etherification of HMF. Interestingly, a small amount of metallic Cu could largely facilitate the hydrogenation of aldehyde group in HMF. In this context, we further proposed a promising two-step strategy for the production of BMMF from fructose in the presence of CuO(5)-USY and Cu, and BMMF yield up to 74.5% was achieved.

2. Experimental

2.1. Materials

$Zr(NO_3)_4{\cdot}5H_2O$, $Zn(NO_3)_2{\cdot}6H_2O$, $Ca(NO_3)_2$, $Ni(NO_3)_2{\cdot}6H_2O$, $Al(NO_3)_3{\cdot}9H_2O$, $Cu(NO_3)_2$ and CuO were purchased from Xilong Chemical Co. Ltd. Methanol, ethanol, isopropanol, n-propanol, n-butanol and dimethylsulfoxide (DMSO) were supplied by Sinopharm Chemical Reagent Co. Ltd in purities of > 99%. Ultra-stable Y zeolite (USY, Si/Al = 14) was obtained from Zibo Xinhong Chemical Trade Co. Ltd. Fructose was purchased from Aladdin Reagent Co. Ltd. 2,5-Bishydroxymethylfuran (BHMF, 95%) and 5-hydroxymethylfurfural (HMF, 98%) were provided by Bepharm Co. Ltd. and Energy Chemical Co. Ltd., respectively.

2.2. Catalyst Preparation

All USY supported metal oxide catalysts were prepared by incipient-wetness impregnation and denoted as M(X)-USY, in which M and X stand for metal oxide and its loading amount (relative to USY zeolite), respectively. In a typical preparation procedure of CuO(5)-USY, 1.179 g $Cu(NO_3)_2$ was added into 6 mL deionized water and stirred at 80 °C until all $Cu(NO_3)_2$ was completely dissolved. The resulting nitrate aqueous solution slowly dripped into 10 g USY zeolite, and then stood overnight at room temperature. The catalyst precursor was dried in oven to remove deionized water followed by calcination for 5 h in a muffle furnace under 400 °C to give CuO(5)-USY catalyst. Also, 2 wt%, 10 wt% or 20 wt% CuO was supported onto USY zeolite by using the above-mentioned method, which were hereafter shown as CuO(2)-USY, CuO(10)-USY and CuO(20)-USY, respectively. In a typical preparation procedure of metallic Cu, 1 g CuO was reduced in a quartz-tube furnace at atmospheric pressure with a flow of H_2/N_2 (1:9) by increasing the temperature from 25 °C to 300 °C and holding for 3 h at 300 °C.

2.3. Characterization

X-ray powder diffraction (XRD) patterns were obtained on a Rigaku Ultima IV diffractometer with Cu-Kα radiation at 40 kV and 30 mA. For scanning electron microscope (SEM) analysis, a SUPRA 55 SAPPHIRE field emission scanning electron microscope at an accelerating voltage of 20 kV was used. Transmission electron microscope (TEM) analysis were performed on a JEM-1400 with an acceleration voltage of 100 kV.

The dispersity of CuO was analyzed on a Micromeritics AutoChem II 2920 using the procedure described by Van Der Grift et al. [39] 0.03 g CuO-USY sample was taken into a U-shaped pyroceram tube and then was first reduced in a 10% H_2/N_2 mixture at a flow rate of 30 mL/min under 450 °C, and the hydrogen consumption (A) was recorded. Then the pyroceram tube was purged with He and cooled down to 50 °C. The oxidation of surface copper atoms to Cu_2O was performed at 50 °C for 0.5 h in a flow of 20% N_2O/N_2 (30 mL/min). Afterwards, the pyroceram tube was flushed with He to remove the oxidant. Finally, the reduction of surface Cu_2O was performed in 10% H_2/N_2 at a flow rate of 30 mL/min, and the amount of hydrogen consumption (B) was recorded. The dispersity (D), the surface area (S) and the average diameter (d) of CuO over USY were calculated according to the followed equations:

$$D = \frac{2 \times B}{A} \times 100\%$$

$$S = \frac{2 \times B \times N_{av}}{A \times M_{Cu} \times 1.4 \times 10^{19}}$$

$$d(nm) = \frac{6}{S \times \rho_{Cu}}$$

Where N_{av}, M_{Cu} and ρ_{Cu} represent Avogadro's constant, the relative atomic mass of copper (63.46 g/mol) and the density of copper (8.92 g/cm^3), respectively. The number of copper atom of per square meter is calculated as 1.4×10^{19}, because the average surface area of copper atom is measured as 7.11×10^{-2} nm^2 [39].

N_2 adsorption-desorption was carried out on a Micromeritics ASAP 2020 sorption analyzer. The mesopore size distribution was obtained by the Barrett-Joyner-Halenda (BJH) model applied to the adsorption

branch of the isotherm. The t-plot method was used to discriminate between micro- and mesoporosity. NH_3 temperature-programmed desorption (NH_3-TPD) and H_2 temperature-programmed reduction (H_2-TPR) were measured on a Micromeritics AutoChem II 2920. A Bruker Tensor 27 spectrometer was used to record Fourier Transform infrared spectroscopy of pyridine (Py-FTIR). In the Py-FTIR experiment, the samples were initially pressed in a self-supporting disc (D = 13 mm), and then reduced at 60 °C for 1 h with subsequent vacuum treatment for 3 h. Pyridine adsorption has been performed by addition of pyridine doses in the cell at room temperature till full saturation of the signal. X-ray photoelectron spectroscopy (XPS) analysis has been performed in a Thermo ESCALAB 250Xi photoelectron spectrometer with monochromated X-ray irradiation Al Kα (hv = 1486.7 eV).

2.4. Typical reactions and product analysis

In this work, all reactions for the formation of furanyl ethers from HMF/fructose were carried out in a Parr autoclave. In a typical experiment for the formation of BMMF from HMF, 0.2 g of HMF, 19.8 g of methanol, 0.1 g of CuO(5)-USY and 0.01 g of metallic Cu were loaded into the reactor. Afterwards, the reactor was sealed and pressurized by 2 MPa of H_2, and then heated to the target temperature with vigorous stirring at 500 rpm. After the reaction, the autoclave was rapidly cooled down to room temperature by running water, and the pressure was then released. Finally, the liquid product was separated by filtration and analyzed by gas chromatography (GC) and gas chromatography-mass spectrometer (GC-MS), respectively. The production of MMF from HMF was performed at the same conditions without H_2 and metallic Cu. One-pot preparation of MMF/BMMF from fructose was conducted by the same procedure using a certain amount of DMSO as a co-solvent.

In a typical two-step reaction of BMMF formation from fructose, a mixture of 0.286 g fructose, 3.0 g DMSO and 0.1 g CuO(5)-USY was loaded into the Parr reactor, and then heated to 130 °C for 3 h to produce HMF in the first step. After the reaction, the autoclave was rapidly cooled down to room temperature by running water. Afterwards, 16.8 g methanol and 0.01 metallic Cu were directly added into the obtained crude HMF product in the reactor, which was sealed and purged with hydrogen three times, and then pressurized by 2 MPa of H_2. The reactor was reheated to 130 °C for 3 h to yield BMMF in the second step. The two-step conversion of fructose to MMF was performed at the same conditions without H_2 and metallic Cu.

We conducted the qualitative and quantitative analysis of products on GC–MS and GC, respectively. HMF conversion (X_{HMF}), product yield ($Y_{Product}$) and selectivity ($S_{Product}$) were calculated using the followed equations:

$$X_{HMF}\,(\mathrm{mol}\,\%) = \left(1 - \frac{\text{moles of detected HMF}}{\text{moles of starting HMF}}\right) \times 100\%$$

$$Y_{Product}\,(\mathrm{mol}\,\%) = \frac{\text{moles of detected product}}{\text{moles of starting HMF}} \times 100\%$$

$$S_{Product} = \frac{\text{product yield}}{\text{HMF conversion}} \times 100\%$$

When using fructose as the starting substrate, product yield was calculated as follows:

$$Y_{Product}\,(\mathrm{mol}\,\%) = \frac{\text{moles of detected product}}{\text{moles of starting fructose}} \times 100\%$$

3. Results and Discussion

3.1. Catalyst Characterization

3.1.1. X-ray diffraction

X-ray diffraction (XRD) profiles of USY supported CuO catalysts display the same set of characteristic diffraction lines in the range of 10° to 35° with respect to pure USY (Fig. 1). What should be paid attention to is that the characteristic peaks of CuO could be clearly observed at 2θ = 35.5° and 38.7° in XRD patterns of CuO(10)-USY and CuO(20)-USY. Nevertheless, no characteristic peak assigned to CuO was visible in the profiles of CuO(5)-USY and CuO(2)-USY, implying the high dispersity of CuO particles in CuO(5)-USY and CuO(2)-USY.

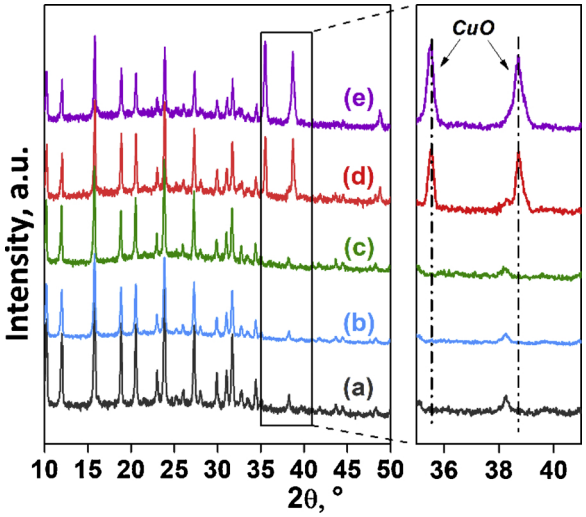

Fig. 1. XRD profiles for pure USY (a), CuO(2)-USY (b), CuO(5)-USY (c), CuO (10)-USY (d) and CuO(20)-USY.

3.1.2. Surface morphology and dispersity of CuO particles

Scanning electron microscope (SEM) and transmission electron microscope (TEM) images of USY zeolite were provided (Fig. S1, a and b), which display that USY zeolite is composed of hierarchical analogues [40]. As shown in Fig. S1c, CuO(5)-USY possesses similar micro morphology to USY parent, which illustrates that the basic framework of USY zeolite remained unchanged after the supporting of CuO. Moreover, elemental mapping of Cu also shows Cu species are uniformly dispersed on the surface of CuO(5)-USY (Fig. S1d).

The size distribution of CuO particles with different loading amount over USY zeolite was analyzed by TEM images in Fig. 2. For all CuO-USY samples, nano-sized CuO particles were dispersed over USY support. The histograms of the particle size distribution are inserted in the bottom-left corner of the corresponding TEM images, suggesting that the diameter of CuO particles increased with the increasing loading of CuO over USY. In the case of CuO(2)-USY, the diameter of the observed CuO particles was concentrated in the range of 1-3 nm. When the CuO loading increased to 5 wt%, the size of CuO particles slightly moves to higher range of 2-4 nm. In comparison, the diameter of CuO particle significantly increased to the ranges of 4-8 nm and 7-11 nm for CuO (10)-USY and CuO(20)-USY, respectively. These above findings indicate that the agglomeration of CuO particles probably occurred with the increase of CuO loading.

The average diameter of CuO particles over CuO-USY catalysts was analyzed and calculated based on TEM, XRD and TPO-TPR characterization technologies. As shown in Table 1, the average size of CuO particles over USY zeolite is highly sensitive to the loading of CuO. For instance, TEM average diameter was calculated from measuring around 100 particles in random fields of TEM view. The TEM average diameter of CuO particles slightly increased from 3.1 to 3.6 nm, with the increase of CuO loading from 2 to 5 wt% (Table 1, entries 1-2). In comparison, the TEM average diameter dramatically increased to 6.5 or 9.1 nm, when the CuO loading was further increased to 10 or 20 wt%, respectively (Table 1, entries 3-4). TPO-TPR characterization also provided a similar variation tendency in the average diameter of CuO with respect to CuO loading. The average diameter of CuO particles for CuO(2)-USY

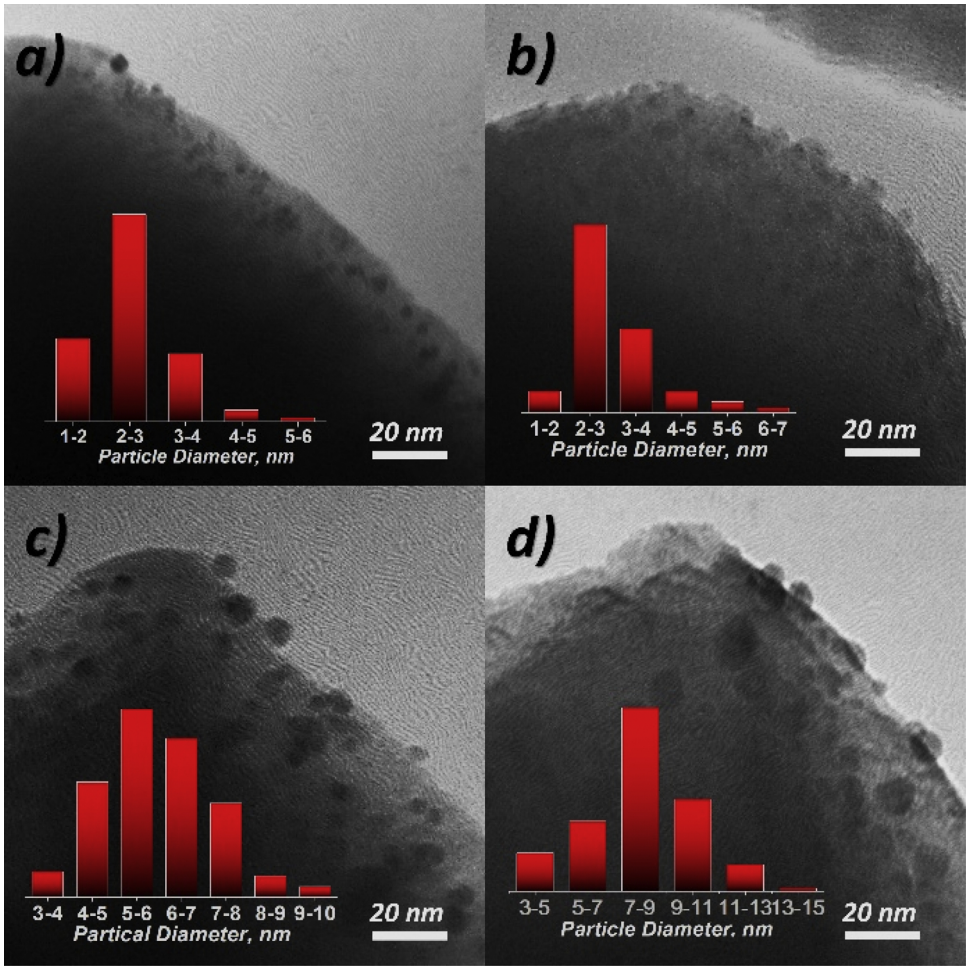

Fig. 2. TEM images and particle distribution of CuO(2)-USY (a), CuO(5)-USY (b), CuO(10)-USY (c) and CuO(20)-USY (d).

Table 1
Average diameter and dispersity of CuO for CuO-USY catalysts.

Entry	Catalyst	CuO average diameter, nm			Dispersity[b], %
		TEM[a]	TPO-TPR[b]	XRD[c]	
1	CuO(2)-USY	3.1	2.7	-	38.1
2	CuO(5)-USY	3.6	2.9	-	36.4
3	CuO(10)-USY	6.5	6.0	5.8	17.3
4	CuO(20)-USY	9.1	8.4	8.3	12.4

[a] Calculated according to $d_{TEM} = \frac{\sum n_i d_i^3}{\sum n_i d_i^2}$, where n_i is the number of particles having a characteristic diameter (d_i) [54].
[b] Calculated method was described in experimental Section 2.3.
[c] Calculated by the Scherrer equation.

and CuO(5)-USY cannot be calculated by Scherrer equation because XRD cannot probe the crystallites of CuO until the CuO loading increased to 10 wt%. The CuO average diameters of CuO(10)-USY and CuO(20)-USY are 5.8 and 8.3 nm, respectively, which are close to those measured by TPO-TPR characterization. The dispersity of CuO over USY zeolite was further calculated. As shown in Table 1, CuO(5)-USY possessed a high dispersity of CuO particles (36.4%) that is comparable to that of CuO(2)-USY (38.1%). On the contrary, the dispersity of CuO particles in CuO(10)-USY or CuO(20)-USY remarkably decreased to 17.3% or 12.4%, respectively. The above findings demonstrated that both the diameter and dispersity of CuO over USY zeolite are highly sensitive to the loading of CuO.

3.1.3. N_2 adsorption-desorption

The N_2 adsorption/desorption isotherms in Fig. S2 show that USY and CuO-USY samples resulted in the characteristic plot for IUPAC type-IV isotherms with H_3-type hysteresis loops, which is consistent with the aggregation of hierarchical porous crystals.[40,41] The distribution diagrams of mesoporous diameter were inserted in the top-left corner of N_2 adsorption/desorption isotherms, where the mesoporous diameter of USY and all CuO-USY samples were concentrated at 3-4 nm (Fig. S2). Table 2 collected the textural properties of USY zeolite and CuO-USY catalysts, including specific surface area, pore volume and micropore volume. USY zeolite possessed a high surface area of 740 m^2/g with a pore volume of 0.37 m^3/g and a micropore volume of 0.23 m^3/g. The surface area, pore volume and micropore volume dropped upon the addition of CuO. For instance, the surface area and pore volume of CuO-USY catalyst gradually decreased from 614 m^2/g

Table 2
Textural properties of USY and CuO-USY catalysts.

Entry	Sample	S.A.[a], m^2/g	V_{pore}[b], cm^3/g	$V_{micropore}$[c], cm^3/g
1	USY	740	0.37	0.23
2	CuO(2)-USY	614	0.33	0.13
3	CuO(5)-USY	595	0.32	0.14
4	CuO(10)-USY	588	0.31	0.19
5	CuO(20)-USY	465	0.25	0.21

[a] Surface area.
[b] Volume adsorbed at $P/P_0 = 0.9999$
[c] By t-plot method.

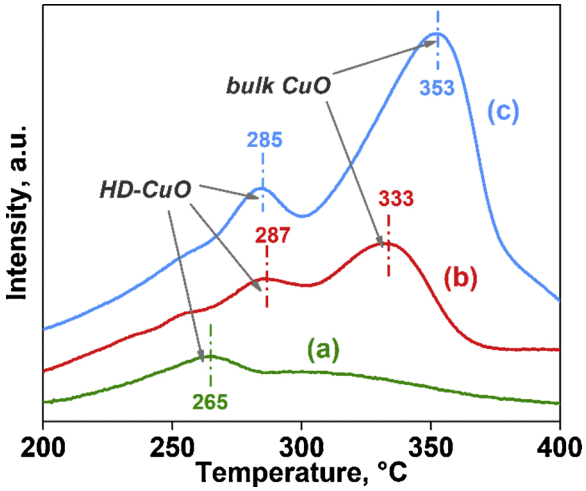

Fig. 3. H_2-TPR profiles of CuO(5)-USY (a), CuO(10)-USY (b) and CuO(20)-USY (c). HD-CuO: highly dispersed CuO.

and 0.33 cm^3/g to 465 m^2/g and 0.25 cm^3/g, respectively, with increasing CuO loading from 2 wt% to 20 wt%. However, with the enhancement of CuO loading, the micropore volume of CuO-USY catalysts increased from 0.13 to 0.21 cm^3/g. Apparently, large-sized CuO particles on the surface of CuO(10)-USY or CuO(20)-USY were beneficial to retain the micropores of USY zeolite.

3.1.4. H_2-TPR

Figs. S3 and 3 illustrate H_2-TPR profiles of pure CuO and CuO-USY catalysts. As shown in Fig. S3, only one peak was observed in the H_2-TPR profile of pure CuO, which could be attributed to the reduction of Cu^{2+} to Cu^0 [42,43]. For CuO-USY catalysts, the intensity of reduction peaks remarkably decreased with the decrease of CuO content. It was found that CuO(10)-USY and CuO(20)-USY had two hydrogen consumption peaks (Fig. 3, b and c), indicating that two kinds of CuO species formed over USY support. To be specific, the peaks centered at lower temperatures (287 and 285 °C) can be assigned to the reduction of highly dispersed CuO (HD-CuO) species over USY support, whereas the peaks around at higher temperatures (333 and 353 °C) can be ascribed to the reduction of bulk CuO species [44]. In addition, with the decrease of CuO loading, the intensity of the peak for the reduction of bulk CuO more sharply decreased as compared to that peak for the reduction of HD-CuO, illustrating that relatively low CuO loading favors the formation of HD-CuO. For example, almost only one peak allocated to the reduction of HD-CuO was observed in the H_2-TPR profile of CuO(5)-USY (Fig. 3, a). This finding is well agree with the average diameter of CuO particles over USY zeolite with varied CuO loading (Table 1).

3.1.5. Surface acidic property

The acidic property of the CuO-USY catalysts was investigated by NH_3-TPD. As shown in Fig. 4A, all catalysts show broad profiles in the range of 100-600 °C, implying the coexistence of weak, moderate and strong acid sites. In this context, these acid sites were quantitated based on peak fitting deconvolution (Fig. S4). As shown in Table 3, the weak and strong acid sites gradually decreased with the increasing CuO content. Nevertheless, the pronounced enhancement in the moderate acid sites was observed with the CuO loading increasing to 5 wt%, rendering the highest total acid sites of 1779.0 μmol/g for CuO(5)-USY (Table 3, entries 2-3). Interestingly, the moderate and total acid sites dramatically reduced to 278.1 and 808.7 μmol/g for CuO(10)-USY (Table 3, entry 4).

To gain more insights into the acidic species of CuO-USY catalysts, Py-FTIR analysis was carried out for these catalysts. As shown in Fig. 4B, the peaks at 1452 and 1543 cm^{-1} can be allocated to Lewis and Bronsted acid sites, respectively, which were quantitated according to fitting deconvolution [45]. As shown in Table 3, USY zeolite had the most Bronsted acid sites of 361.5 μmol/g with negligible Lewis acid sites (Table 3, entry 1). Notably, Lewis acid sites were significantly increased to 457.1 μmol/g at the cost of Bronsted acid sites (219.9 μmol/g) in the case of CuO(5)-USY (Table 3, entry 3). Incredibly, both Lewis and Bronsted acid sites steeply decreased to 53.6 and 7.9 μmol/g, respectively if the CuO loading increased to 10 wt% in CuO(10)-USY (Table 3, entry 4). This observation is in good agreement with the results of NH_3-TPD, indicating that the introduction of CuO onto USY zeolite brought about moderate Lewis acid sites (Table 3). Partial Al-OH species on the surface of USY zeolite could be transformed into Al-O-Cu^{2+} species in CuO-USY catalysts (discussed in details in XPS analysis), new Lewis acid sites thus generated at the cost of Bronsted acid sites over USY zeolite. In this context, highly dispersed CuO particles over CuO(2)-USY or CuO(5)-USY could offer plenty of Lewis acid sites (Al-O-Cu^{2+} species), whereas bulk CuO particles over CuO(10)-USY brought about a small amount of Lewis acid sites at the cost of Bronsted acid sites.

3.1.6. XPS analysis

The electronic state of elements on the surface of CuO(5)-USY catalysts was characterized by XPS (Figs. 5A and S5). As shown in Fig. 5A(a), $Cu2p_{3/2}$ and $Cu2p_{1/2}$ of pure CuO show binding energies (BE) around at 933 and 953 eV, respectively, disclosing that only Cu(II) species existed in pure CuO. The detected peak at a BE region between 938 and 948 eV can be attributed to the satellite of Cu(II) species. In comparison, a careful deconvolution of either $Cu2p_{3/2}$ or $Cu2p_{1/2}$ for CuO(5)-USY shows an additional shoulder peak at higher BE ranges (Fig. 5A(b)), which is probably attributed to the formation of Al-O-Cu (II) species by the strong interaction between Cu(II) species and USY support.[46–48] Indeed, such a shift of BE for the Cu(II) species is characteristic of a charge transfer from Cu^{2+} towards the USY support [49]. As observed from Fig. S5, both Si2p and O1s XPS signals of CuO (5)-USY can be fitted by one Gaussian peak, while the XPS signal for the Al2p shows an unsymmetrical profile that can be fitted by two Gaussian peaks, which should be assigned to Si-O-Al-OH and Si-O-Al-O-Cu(II) species, respectively, suggesting the charge transfer from Cu^{2+} towards support aluminum through oxide as a bridge. It is known that the Bronsted acidity of USY zeolite results from the surface OH groups (Al-OH), which are formed for balancing the charge on the zeolite framework induced by the presence of aluminum [50]. The number of OH groups on the surface of USY support decreased after Cu^{2+}/H^+ exchange (Fig. 5B) [51]. Hence, Lewis acid sites (surface Cu^{2+} species) generated at the cost of Bronsted acid sites via the formation of Al-O-Cu (II) species after the introduction of CuO onto the surface of USY, which is in good agreement with the characterization of Py-FTIR (Table 3).

3.2. Etherification of HMF over CuO-USY

The effect of USY supported metal oxides on product distribution was examined initially in isopropanol under 120 °C and for 3 h. As shown in Table 4,and 5-hydroxymethylfurfural diisopropylacetal (HMFDPA) and 5-isopropoxymethylfurfural (PMF) were detected as the main products in the most of tests, which formed by the acetalation and etherification of HMF with isopropanol over Brønsted and Lewis acid sites, respectively. However, ZnO(5)-USY and CaO(5)-USY showed negligible catalytic activity for the conversion of HMF in isopropanol (Table 4, entries 1 and 2). NiO(5)-USY provided a HMF conversion of 35.8% with 2,5-bishydroxymethylfuran (BHMF) and PMF as the main products (Table 4, entry 3), indicating that NiO(5)-USY is capable of catalyzing the etherification and MPV reduction reaction of HMF. The HMF and PMF selectivity were further improved to 49.1%, 78.2% and 60.3%, 59.6% over Al_2O_3(5)-USY or ZrO_2(5)-USY, respectively (Table 4, entries 4 and 5). Intriguingly, CuO(5)-USY afforded complete consumption of HMF and a high PMF selectivity up to 94.9% with a

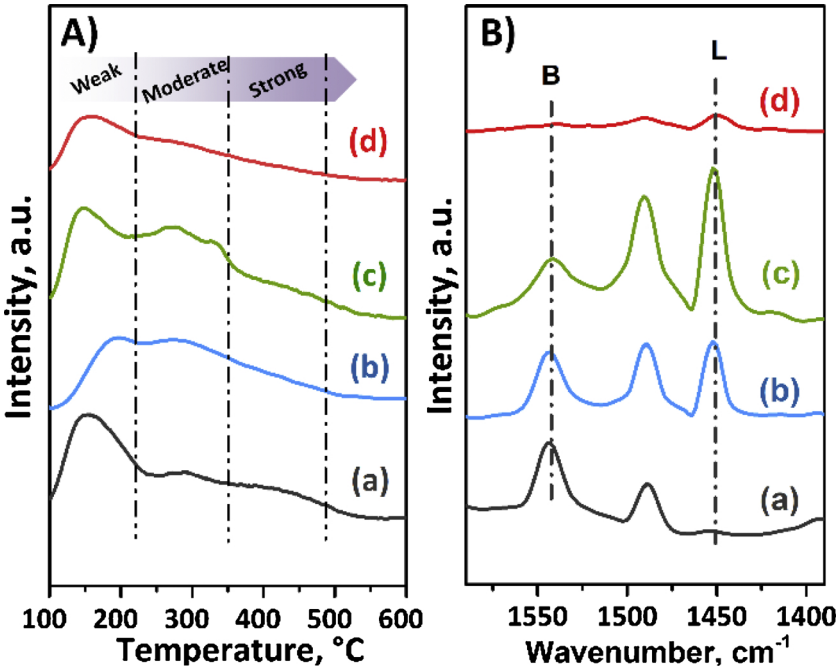

Fig. 4. NH_3-TPD profiles (A) and Py-FTIR spectra (B) of USY zeolite (a), CuO(2)-USY (b), CuO(5)-USY (c) and CuO(10)-USY (d).

high TOF of 25.3 h^{-1} under the same conditions (Table 4, entry 6), reflecting the highest activity compared to other USY supported metal oxides (Table 4, entries 1-5). If the reaction was catalyzed by a mixture of USY zeolite and copper oxide, low HMF conversion (19.2%) with no PMF was achieved (Table 4, entry 7), which implies that the dispersity of CuO over USY support has a crucial effect on the catalytic performance of the catalyst. The superior catalytic performance of CuO(5)-USY should be attributed to the abundance of acid sites over CuO(5)-USY with highly dispersed CuO particles (Tables 2 and 4).

Given the superior catalytic performance of CuO-USY, the effect of loading amount of CuO over USY zeolite on product distribution was further investigated (Fig. 6). In the case of pure USY zeolite, HMF conversion of 29.4% with negligible PMF was achieved (Table 4, entry 8), implying USY zeolite with Bronsted acid sites is not able to effectively catalyze HMF etherification under the applied conditions. Interestingly, both HMF conversion and PMF selectivity were remarkably improved to 76.7% and 80.8% over CuO(2)-USY, which further increased to 100% and 94.9%, respectively over CuO(5)-USY under the same reaction conditions. However, HMF conversion and PMF selectivity sharply decreased to 44.8% and 59.0%, respectively in the presence of CuO(10)-USY. This above finding is in good consistent with the amount for Lewis acid sites in CuO-USY catalysts (Table 4), indicating that Lewis acid sites resulting from the introduction of CuO greatly facilitated the etherification of HMF with isopropanol to give PMF.

The etherification of HMF to yield 5-alkoxymethylfurfurals (AMFs) also relies on the experimental alcohol solvents. It should be noted that the steric hindrance (SH) of alcohols has significant influence on the formation of ethers. To evaluate the effect of the SH of alcohols on the product selectivity, the etherification of HMF was conducted in a mixture of C1-C4 alcohols at 120 °C in 3 h. For all studied n-alcohols, the AMFs selectivity decreased with the increase of the SH value of corresponding n-alcohol. As shown in Fig.7, the SH value of n-alcohols increases in the order of methanol (1.986 kcal/mol) < ethanol (2.813 kcal/mol) < n-propanol (4.116 kcal/mol) < n-butanol (4.688 kcal/mol), which resulted in AMFs selectivities decreasing in the order of 5-methoxymethylfurfural (MMF, 48.3%) > EMF (22.8%) > 5-propoxymethylfurfural (n-PMF, 8.5%) > 5-butoxymethylfurfural (n-BMF, 5.2%). Interestingly, isopropanol with a lower SH offered a relatively low PMF selectivity (4.8%) versus to n-PMF, demonstrating that HMF might be more difficult to react with sec-alcohols. At this point, one can thus conclude that methanol is a preferable solvent for the etherification of HMF over CuO(5)-USY as compared to other alcohols.

In addition, the etherification of HMF was conducted in different n-alcohols individually over CuO(5)-USY at 100-120 °C in 3 h, and desirable AMF yields were obtained in all the cases (Table S1). As expected, methanol gave a MMF yield up to 98.3% at a relatively low temperature (100 °C) within 3 h (Table S1, entry 1). Ethanol gave a EMF yield as high as 96.9% at 110 °C in 3 h (Table S1, entry 2). Moreover, a

Table 3
Composition of acid sites for USY zeolite and CuO-USY catalysts.

Entry	Catalyst	Acid sites, μmol/g						
		Weak[a]	Moderate[a]	Strong[a]	Total	Lewis[b]	Bronsted[c]	"L + B"[d]
1	USY	573.8	350.0	309.2	1233.0	9.1	361.5	370.6
2	CuO(2)-USY	508.6	532.6	296.5	1337.7	247.3	335.9	583.2
3	CuO(5)-USY	431.3	1124.3	223.4	1779.0	457.1	219.9	607.0
4	CuO(10)-USY	335.3	278.1	195.3	808.7	53.6	7.9	61.5

[a] Calculated by fitting deconvolution of peaks in Fig. S4; weak acid sites are the sum of weak 1 and weak 2.
[b] Calculated by fitting deconvolution of peaks assigned to Lewis acidity in Fig. 4B.
[c] Calculated by fitting deconvolution of peaks assigned to Bronsted acidity in Fig. 4B.
[d] The sum of Lewis and Bronsted acid sites.

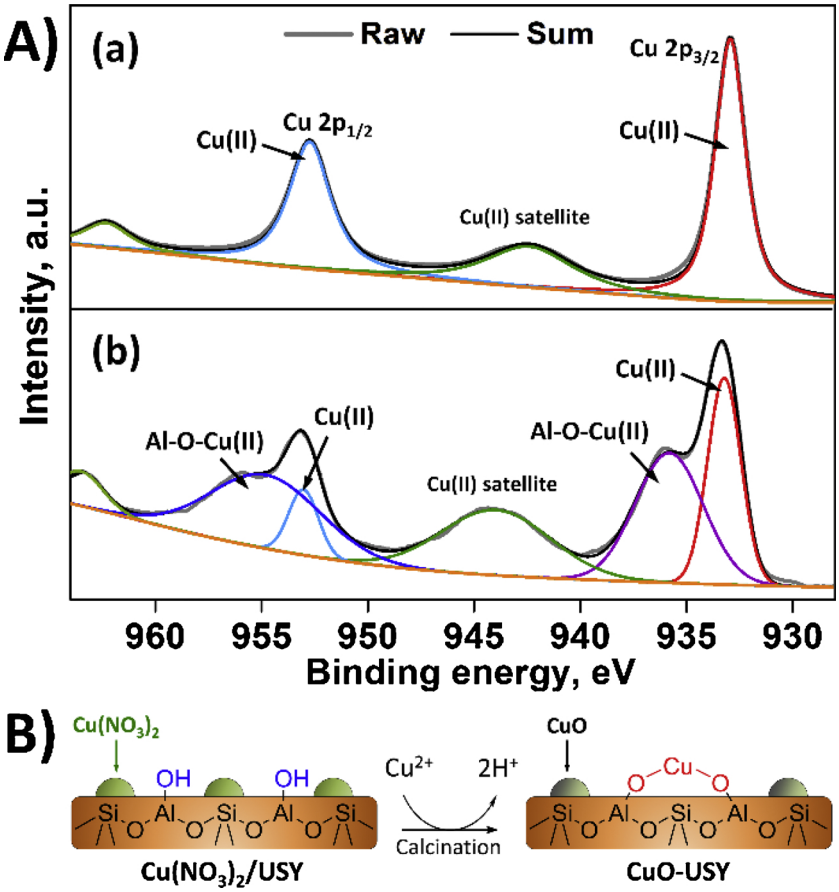

Fig. 5. A) XPS spectra of pure CuO (a) and CuO(5)-USY (b); B) The Cu^{2+}/H^{+} exchange on the surface of USY in the procedure of calcination.

n-PMF yield of 95.9% and a n-BMF yield of 91.5% were achieved at 120 °C in 3 h in the presence of CuO(5)-USY (Table S1, entries 3-4). Therefore, a family of C8-C10 mono-ethers could be readily prepared in high yields over CuO(5)-USY.

3.3. Reductive etherification of HMF in methanol

It is highly desirable to produce BAMFs by the reductive etherification of HMF, because they have high energy density and greater miscibility with commercial diesel than mono-ethers [18,19]. To this end, the reductive etherification of HMF was performed in methanol under H_2 atmosphere (Table 5). However, USY and CuO(5)-USY still gave 5-hydroxymethylfurfural dimethylacetal (HMFDMA) and MMF as the dominant product without BMMF at 90 °C in 3 h under H_2 atmosphere (Table 5, entries 1 and 2), implying that USY and CuO(5)-USY are not able to catalyze the hydrogenation of HMF. Many metallic Cu catalysts were served as active catalysts for the HMF hydrogenation [38], Cu(5)-USY was thus prepared by the reduction of CuO(5)-USY at

Table 4
. Catalytic performance of USY supported metal oxides in HMF etherification in isopropanol.[a]

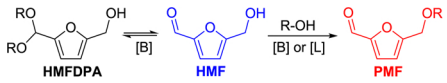

Entry	Catalyst[b]	X_{HMF}, %	TOF[c], h^{-1}	Selectivity of products, %	
				PMF	HMFDPA
1	ZnO(5)-USY	2.6	-	n.d	n.d
2	CaO(5)-USY	0.5	-	n.d	n.d
3[d]	NiO(5)-USY	35.8	4.2	42.7	n.d
4	Al_2O_3(5)-USY	49.1	7.9	60.3	16.3
5	ZrO_2(5)-USY	78.2	15.3	59.6	29.8
6	CuO(5)-USY	100.0	25.3	94.9	0.5
7	USY + CuO[e]	19.2	-	n.d	89.6
8	USY	29.4	-	2.6	93.3

[a] Reaction conditions: 120 °C, 3 h, 0.2 g HMF, 19.8 g isopropanol and 0.1 g catalyst; n.d: not detected.
[b] The SiO_2/Al_2O_3 mole ratio of USY zeolite is 14.
[c] The "TOF" value was calculated based on the content of active metal oxides in the same conversion level (around 10%).
[d] A BHMF selectivity of 38.0% was obtained.
[e] The dosages of USY and CuO are equal to those in 0.1 g CuO(5)-USY.

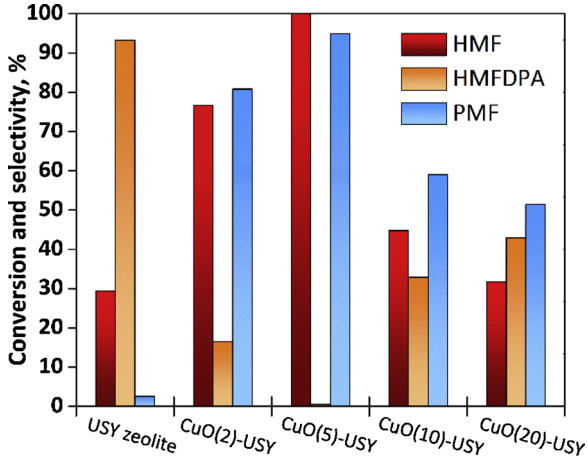

Fig. 6. Effect of the CuO loading on the catalytic performance in HMF etherification. Reaction conditions: 120 °C, 3 h, 0.2 g HMF, 0.1 g catalyst and 19.8 g isopropanol.

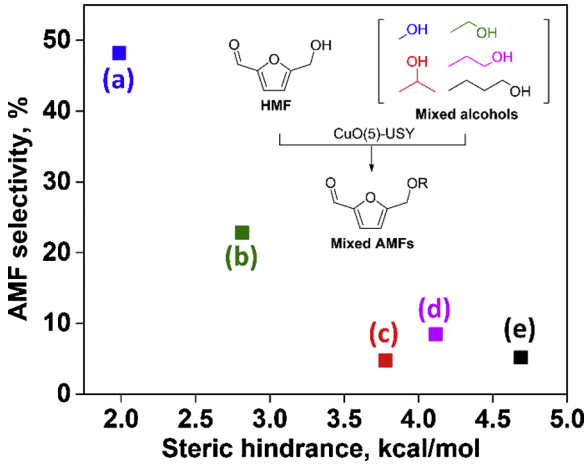

Fig. 7. Effect of steric hindrance of alcohols on the etherification of HMF to AMFs with methanol (a), ethanol (b), isopropanol (c), n-propanol (d) and n-butanol (e). Reaction conditions: 120 °C, 3 h, 0.5 g HMF, 0.2 g CuO(5)-USY and 50.0 g mixed alcohols (each alcohol is 10.0 g).

Table 5
. Coupled hydrogenation and etherification of HMF in methanol[a]

Entry	Catalyst	T, °C	X_{HMF}, %	Selectivity, %		
				HMFDMA	MMF	BMMF
1	USY	90	13.8	100.0	n.d	n.d
2	CuO(5)-USY	90	92.0	7.8	92.1	n.d
3	Cu(5)-USY	90	43.6	56.2	6.9	26.1
4	CuO(5)-USY + Cu	90	100.0	n.d	31.8	68.1
5	CuO(5)-USY + Cu	100	100.0	n.d	25.1	74.3
6	CuO(5)-USY + Cu	110	100.0	n.d	14.6	84.0
7	CuO(5)-USY + Cu	120	100.0	n.d	5.9	92.2
8	CuO(5)-USY + Cu	130	100.0	n.d	n.d	95.3

[a] Reaction conditions: 0.2 g HMF, 19.8 g methanol (R-OH), 0.1 g USY/CuO (5)-USY/ Cu(5)-USY, 0.01 g Cu, 3 h and 2 MPa H_2; n.d: not detected.

300 °C for 2 h under H_2 flow (10 vol% H_2/N_2). Although, BMMF selectivity of 26.1% was achieved over Cu(5)-USY at the same conditions, HMF conversion sharply decreased to 43.6% with HMFDMA formed by the acetalation of HMF as the main product (Table 5, entry 3). The poor catalytic activity for the etherification of HMF over Cu(5)-USY should be probably attributed to the partial loss of Lewis acid sites (Cu^{2+} species) during the reduction process of CuO.

In order to produce BMMF with high selectivity, a combination of CuO(5)-USY and metallic Cu powder was examined for the reductive etherification of HMF under H_2 atmosphere in methanol. As expected, the Cu-based mixed catalysts offered a 100% HMF conversion with an improved BMMF selectivity of 68.1% at 90 °C in 3 h under H_2 atmosphere (Table 5, entry 4). The BMMF selectivity gradually increased to 95.3% at the cost of MMF selectivity in the presence of the Cu-based mixed catalysts if the reaction temperature further increased to 130 °C within 3 h (Table 5, entries 5-8). Notably, only MMF and BMMF were detected in the products derived from the reductive etherification of HMF over the Cu-based mixed catalyst system, and both of them can be employed as potential bio-diesel additives. Therefore, it is flexible to produce a mixture of MMF and BMMF at relatively moderate conditions, or to obtain BMMF with high yield at relatively high temperature in the presence of Cu-based mixed catalyst system.

A plausible reaction pathway for the reductive etherification of HMF to BMMF in the presence of Cu-based mixed catalysts was proposed in Scheme 1. Given that the "CuO(5)-USY + Cu" catalytic system has superior catalytic activity for both hydrogenation and etherification reactions, there is thus two possible routes for the reductive etherification of HMF to BMMF (Scheme 1). In the route 1, HMF first undergoes the etherification with methanol to form MMF, which could be further reduced to 2- hydroxymethyl-5-methoxymethylfuran (HMMF) followed by the etherification to give BMMF. In the route 2, HMF is first subjected to the hydrogenation to BHMF, which could be converted to BMMF through HMMF as the intermediate by two successive etherification reactions. Notably, 100% HMF conversion with no BHMF or HMMF was achieved in all the tests in Table 5, indicating that the etherification of HMF, BHMF or HMMF is a fast step over these Cu-based catalysts under the applied conditions.

To gain more insights into the reaction pathway of the reductive etherification of HMF over the Cu-based mixed catalyst, we compared the reaction rate between the etherification over CuO(5)-USY and the hydrogenation over metallic Cu at the same conditions (90 °C). As shown in Fig. 8, the reaction rate for the etherification of BHMF is slightly higher than that of HMF catalyzed by CuO(5)-USY. In addition, the hydrogenation of HMF shows a slightly higher reaction rate as compared to that of the hydrogenation of MMF in the presence of metallic Cu. However, the reaction rate for the etherification of HMF over CuO(5)-USY is much higher than that for the hydrogenation of HMF over metallic Cu (Fig. 8). It is known that CuO(5)-USY has no hydrogenation activity under hydrogen atmosphere (Table 5, entry 2), and metallic Cu is not able to promote the etherification reaction. Therefore, CuO(5)-USY and Cu are independently responsible for the etherification and hydrogenation reactions, respectively in the mixed catalyst system. One can thus infer that the reductive etherification of HMF in methanol preferentially undergoes the route 1 (Scheme 1) to BMMF in the presence of CuO(5)-USY and Cu. On the other hand, a spot of generated BHMF could be instantly etherified to HMMF or BMMF, because of the high reaction rate for BHMF etherification over CuO(5)-USY (Fig. 8). Hence, the hydrogenation of MMF is the rate limiting step for BMMF formation by the reductive etherification of HMF over Cu-based mixed catalyst system, due to the relatively low hydrogenation rate of MMF over metallic Cu (Fig. 8).

Excitingly, this Cu-based mixed catalyst system is also well applicable to the production of a spectrum of BAMFs in other C2-C4 alcohols. As shown in Table S2, the desirable yields of 2, 5-bis(ethoxymethyl) furan, 2, 5-bis(isopropoxymethyl)furan, 2, 5-bis(propoxymethyl)furan and 2, 5-bis(butoxymethyl)furan were offered as 92.4%, 81.4%, 80.2% and 76.5%, respectively under the optimized reaction conditions.

3.4. Catalyst recirculation

The stability of catalysts is of great importance for the practical application; thus, the recycling tests of Cu-based catalysts were carried out in methanol. In this study, the spent catalyst was recycled from the

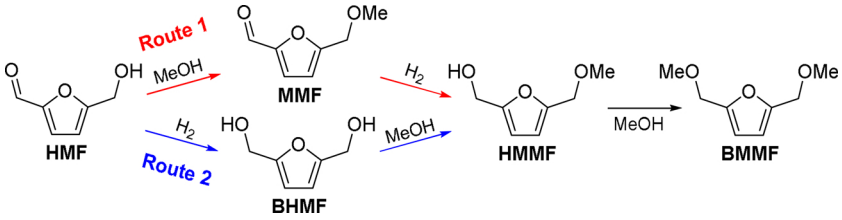

Scheme 1. A plausible reaction pathway for the reductive etherification of HMF to BMMF.

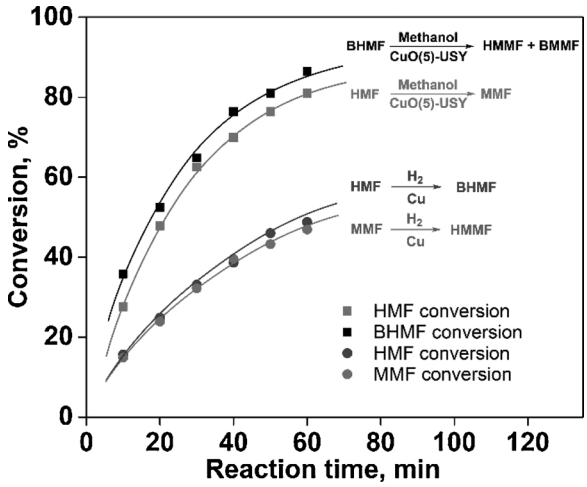

Fig. 8. Comparison of reaction rate between the etherification reaction over CuO(5)-USY and the hydrogenation reaction over metallic Cu. Etherification reaction conditions: 0.2 g HMF/BHMF, 19.8 g methanol, 0.1 g CuO(5)-USY, 90 °C and 2 MPa N_2. Hydrogenation reaction conditions: 0.2 g HMF/MMF, 19.8 g methanol, 0.01 g Cu, 90 °C and 2 MPa H_2.

solution by filtration in vacuum after reaction and washed with methanol three times, then the resulting catalyst was dried at 100 °C for 2 h before being put into the next cycle. As shown in Fig. 9A, both HMF conversion and MMF selectivity nearly kept unchanged for the etherification of HMF over CuO(5)-USY in methanol after five cycles. The possible leaching of Cu species from CuO(5)-USY was also measured by ICP-OES, which suggested that negligible Cu species (less than 0.1% relative to the molar weight of Cu in the fresh catalyst) were detected in the liquid product obtained from the etherification of HMF over CuO (5)-USY. Elemental analysis demonstrated that no carbon deposit was detected in the spent CuO(5)-USY recovered from the fifth cycle, suggesting that almost no furanyl ether covered the active sites and/or blocked the pores of catalysts. Therefore, the spent CuO(5)-USY recovered from the fifth cycle possessed comparable acid sites and BET surface area to those of the fresh one (Fig. S6, a and c). Besides, almost the same XRD profiles for the fresh catalyst and spent catalyst recovered from the fifth cycle were observed. Based on the above observations, CuO(5)-USY acted as an efficient and robust catalyst for the etherification of HMF in methanol.

Recycling tests of the combination of CuO(5)-USY and Cu for the reductive etherification of HMF was also conducted using the same strategy. As can be seen from Fig. 9B, HMF conversion and the total selectivity of BMMF and MMF almost remained constant even after the fifth reuse of the combined Cu-based catalyst. However, the selectivity of BMMF decreased considerably from 74.3% to 37.9%, whereas MMF selectivity increased from 25.1% to 59.0 % after the fifth reuse of the combined Cu-based catalyst. Given only a small amount of Cu powder (0.01 g) in the combined Cu-based catalysts, it is reasonable that the partial loss of metallic Cu is inevitable during the recycling of the combined Cu-based catalysts. Therefore, the partial loss of metallic Cu should mainly responsible for the decrease in the catalytic activity of the combined Cu-based catalyst for the hydrogenation of MMF. For the mixed Cu catalysts containing Cu-USY and metallic Cu, it is infeasible to measure the loss of metallic Cu with the recycling test of the mixed Cu catalysts. To verify the above assumption, the recycling tests of metallic Cu for the hydrogenation of HMF were conducted (Table S3). It was found that BHMF selectivity of 100.0% was achieved in every catalytic cycle while the HMF conversion and the recycling mass of metallic Cu gradually decreased to 31.7% and 0.0040 g after five cycles,

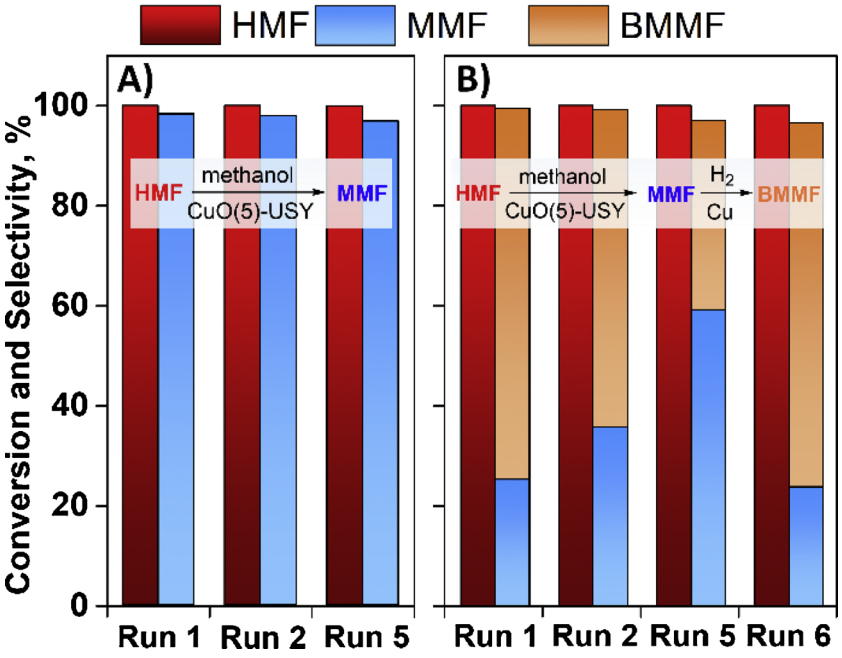

Fig. 9. Recycled experiments for the etherification of HMF over CuO(5)-USY (A) and the reductive etherification of HMF over a combination of CuO(5)-USY and Cu (B). Reaction conditions: 0.2 g HMF, 19.8 g methanol, 0.1 g CuO(5)-USY, 100 °C, 3 h, 2 MPa H_2, and 0.01 g Cu added to the reductive etherification reactions. Another 0.01 g Cu was added in 6th run.

Table 6
. One-pot conversion of fructose to furanyl ethers in methanol[a]

Entry	Catalyst	Solvent composition	Yield, %			
			HMF	MMF	ML	BMMF
1	CuO(5)-USY	100 wt% methanol	n.d	14.1	5.3	n.d
2	CuO(5)-USY	50 wt% DMSO	n.d	35.4	1.4	n.d
3	CuO(5)-USY	67 wt% DMSO	n.d	50.5	n.d	n.d
4	CuO(5)-USY	75 wt% DMSO	1.8	56.9	n.d	n.d
5	CuO(5)-USY	80 wt% DMSO	15.2	37.0	n.d	n.d
6[b]	CuO(5)-USY + Cu	75 wt% DMSO	n.d	n.d	n.d	47.3

[a] Reaction conditions: 0.286 g fructose, 0.1 g CuO(5)-USY, 19.8 g solvent, 130 °C and 3 h; n.d: not detected.
[b] 0.286 g fructose, 0.1 g CuO(5)-USY, 0.01 g Cu, 19.8 g solvent, 130 °C, 2 MPa H_2 and 3 h.

respectively. The HMF conversion recovered in the sixth cycle if another 0.0060 g spent metallic Cu from the fifth cycle was added into the reaction, suggesting that the decrease in the hydrogenation activity is mainly caused by the partial loss of metallic Cu. In this context, another 0.01 g Cu was added into the spent combined Cu-based catalyst and reused in the sixth recycling test. As expected, BMMF selectivity recovered to the similar level to that obtained in the presence of the fresh combined Cu-based catalysts (Fig. 9B).

3.5. Conversion of fructose to furanyl ethers

In light of USY zeolite having plenty of Bronsted acid sites (Table 3, entry 1), the catalytic performance of USY zeolite for the dehydration of fructose to HMF was evaluated. We first performed the acid-catalyzed dehydration of fructose in DMSO. As expected, CuO(5)-USY gave a desirable HMF yield of 86.2% at 130 °C in 3 h. In comparison, USY zeolite only offered a moderate HMF yield of 56.3% from fructose at the same conditions, which indicates that Lewis acid sites resulted from the introduction of CuO in CuO(5)-USY greatly promoted the dehydration of fructose to HMF. This finding suggests that CuO(5)-USY could serve as a highly efficient catalyst for both fructose dehydration and HMF etherification.

Encouraged by the above findings, we further investigated the one-pot conversion of fructose into furanyl ethers in methanol. However, a MMF yield of only 14.1% with no HMF was obtained from fructose over CuO (5)-USY in methanol at 130 °C for 3 h (Table 6, entry 1). Notably, a black liquid product with a small amount of methyl levulinate (ML) was obtained in this case, indicating that the most of fructose probably converted into by-products like humins in the presence of CuO(5)-USY in methanol. Interestingly, the MMF yield pronouncedly increased with the addition of DMSO in methanol at the same conditions. For example, a MMF yield of 35.4% was achieved from fructose in 50 wt% DMSO methanol solution (Table 6, entry 2), which further increased to 56.9% in 75 wt% DMSO methanol solution (Table 6, entry 4). The solvation of HMF by DMSO probably occurred, which could keep the resulting HMF from the side-reactions to form humins [52], and then facilitated the etherification of HMF to MMF. On the other hand, the introduction of DMSO could promote the dissociation of methanol to provide a more acidic environment [53], which is also beneficial to the acid-catalyzed dehydration of fructose to HMF and the subsequent etherification to MMF.

Nevertheless, further increasing DMSO content to 80 wt% resulted in a significant decrease in the MMF yield (37.0%) with an improved HMF yield of 15.2% (Table 6, entry 5). Apparently, the relatively low methanol concentration was also detrimental to the etherification of HMF in this case. In addition, a combination of CuO(5)-USY and metallic Cu could give a BMMF yield of 47.3% starting from fructose at 130 °C for 3 h in 75 wt% DMSO methanol solution (Table 6, entry 6). Note that this is the first report on the one-pot conversion of fructose to BMMF with a moderate yield.

To further increase the furanyl ethers yield from fructose, a facile two-step strategy was proposed based on the Cu-based catalyst system in this study. As shown in Scheme 2, the initial dehydration of fructose was conducted at 130 °C for 3 h over CuO(5)-USY in pure DMSO, giving a desirable HMF yield of 86.2%. Then, methanol was directly added into the obtained crude HMF product. As for the MMF production, the resulting mixture was reheated to 100 °C for another 3 h to give a MMF yield up to 79.6% based on fructose, which is the highest MMF yield to date starting from fructose over a heterogeneous catalyst. Excitingly, BMMF yield as high as 74.5% based on fructose was also achieved if extra 0.01 g metallic Cu was introduced and the resulting mixture reacted at 130 °C for another 3 h under 2 MPa H_2. Therefore, it is flexible to afford MMF or BMMF with desirable yield from fructose in the presence of the Cu-based catalyst system.

4. Conclusions

In this work, a flexible Cu-based catalyst system consisting of CuO-USY or with metallic Cu was proposed for the transformation of fructose to furanyl ethers, such as 5-alkoxymethylfurfurals (AMFs) and 2,5-bis (alkoxymethyl)furans (BAMFs), as potential bio-fuels. The dispersity of CuO over CuO-USY catalyst could be manipulated by adjusting the loading of CuO. Specifically, relatively low CuO loading favored the formation of highly dispersed CuO, and Lewis acid sites generated at the cost of Bronsted acid sites by the formation of Al-O-Cu(II) species. Among CuO-USY catalysts with varied CuO loading, CuO(5)-USY with an abundance of acid sites exhibited superior catalytic performance for both fructose dehydration and the etherification of HMF. Moreover, a small amount of metallic Cu could effectively facilitate the hydrogenation of HMF and 5-alkoxymethylfurfurals (AMFs) under hydrogen atmosphere. In this context, a family of AMFs or BAMFs can be produced from fructose by a facile two-step strategy in a flexible Cu-based catalyst system. For instance, 5-methoxymethylfurfural (MMF) up to 79.6% was achieved over CuO(5)-USY by the dehydration of fructose in DMSO and the subsequent etherification of HMF in DMSO/methanol mixture. Excitingly, 2,5-bis(methoxymethyl)furan (BMMF) yield as high as 74.5% was also obtained from fructose by the dehydration and the subsequent reductive etherification in the presence of CuO(5)-USY and Cu.

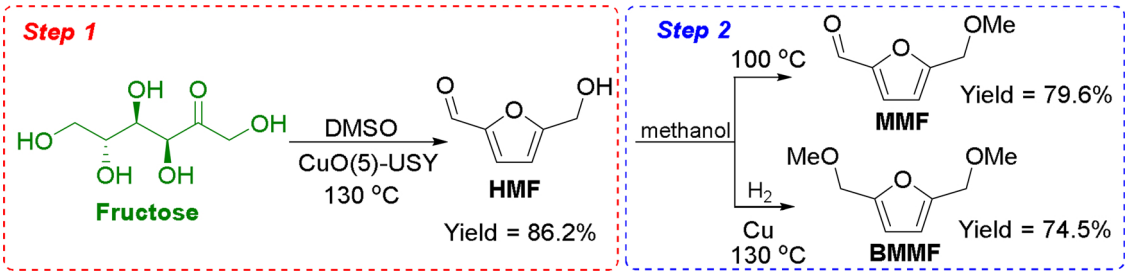

Scheme 2. The preparation of MMF/BMMF from fructose by a two-step strategy. Reaction conditions for step 1: 0.286 g fructose, 3.0 g DMSO, 0.1 g CuO(5)-USY, 130 °C and 3 h. Reaction conditions for step 2: 16.8 g methanol, 100 °C and 3 h for MMF production; extra 0.01 g Cu, 130 °C and 2 MPa H_2 for BMMF formation.

Acknowledgements

We are grateful for funding supported by the National Natural Science Foundation of China (Grant Nos. 21706223; 21776234; 21676223), the Natural Science Foundation of Fujian Province of China (Grant Nos. 2018J01017), the Education Department of Fujian Province (Grant No. JZ160398) and the Energy Development Foundation of Energy College, Xiamen University (Grant No. 2017NYFZ02).

Appendix A. Supplementary data

Supplementary material related to this article can be found, in the online version, at doi:https://doi.org/10.1016/j.apcatb.2019.117793.

References

[1] S.K. Maity, Renewable Sustainable Energy Rev. 43 (2015) 1427–1445.
[2] R. Rinaldi, F. Schüth, ChemSusChem 3 (2010) 1096–1107.
[3] Q. Hou, M. Zhen, W. Li, L. Liu, J. Liu, S. Zhang, Y. Nie, C. Bai, X. Bai, M. Ju, Appl. Catal., B 253 (2019) 1–10.
[4] X. Tang, X. Zeng, Z. Li, L. Hu, Y. Sun, S. Liu, T. Lei, L. Lin, Renewable Sustainable Energy Rev. 40 (2014) 608–620.
[5] F. Li, L.J. France, Z. Cai, Y. Li, S. Liu, H. Lou, J. Long, X. Li, Appl. Catal. B 214 (2017) 67–77.
[6] Y. Romanleshkov, C.J. Barrett, Z.Y. Liu, J.A. Dumesic, Nature 447 (2007) 982–985.
[7] J. Lange, W.D.V. De Graaf, R.J. Haan, ChemSusChem 2 (2009) 437–441.
[8] B. Liu, Z. Zhang, ChemSusChem 47 (2016) 2015–2036.
[9] K.S. Arias, M.J. Climent, A. Corma, S. Iborra, ChemSusChem 7 (2014) 210–220.
[10] P. Che, F. Lu, J. Zhang, Y. Huang, X. Nie, J. Gao, J. Xu, Bioresour. technol. 119 (2012) 433–436.
[11] P. Lanzafame, D.M. Temi, S. Perathoner, G. Centi, A. Macario, A. Aloise, G. Giordano, Catal. Today 175 (2011) 435–441.
[12] E.R. Sacia, M. Balakrishnan, A.T. Bell, J. Catal. 313 (2014) 70–79.
[13] J. Wei, X. Cao, T. Wang, H. Liu, X. Tang, X. Zeng, Y. Sun, T. Lei, S. Liu, L. Lin, Catal. Sci. Technol. 8 (2018) 4474–4484.
[14] M. Mascal, E.B. Nikitin, Angew. Chem. Int. Ed. 47 (2010) 7924–7926.
[15] M. Mascal, S. Dutta, Green Chem. 13 (2010) 40–41.
[16] Y. Dou, M. Zhang, S. Zhou, C. Oldani, W. Fang, Q. Cao, Eur. J. Inorg. Chem. 2018 (2018) 3706–3716.
[17] F. Yang, S. Zhang, Z.C. Zhang, J. Mao, S. Li, J. Yin, J. Zhou, Catal. Sci. Technol. 5 (2015) 4602–4612.
[18] G.J.M. Gruter, Mixture of furfural and 5-(alkoxymethyl) furfural derivatives from sugars and alcohols, European Patent, 2012.
[19] E. de Jong, T. Vijlbrief, R. Hijkoop, G.-J.M. Gruter, J.C. van der Waal, Biomass Bioenergy 36 (2012) 151–159.
[20] Q. Cao, W. Liang, J. Guan, L. Wang, Q. Qu, X. Zhang, X. Wang, X. Mu, Appl. Catal., A 481 (2014) 49–53.
[21] H. Nguyen, N.L. Xiao, S. Daniels, N. Marcella, J. Timoshenko, A.I. Frenkel, D.G. Vlachos, Acs Catal. 7 (2017) 7363–7370.
[22] J. Wei, T. Wang, H. Liu, M. Li, X. Tang, Y. Sun, X. Zeng, L. Hu, T. Lei, L. Lin, Energy Technol. 7 (2019) 1801071.
[23] S. Shinde, C. Rode, ChemSusChem 10 (2017) 4090–4101.
[24] J.D. Lewis, S. Van de Vyver, A.J. Crisci, W.R. Gunther, V.K. Michaelis, R.G. Griffin, Y. Román-Leshkov, ChemSusChem 7 (2014) 2255–2265.
[25] J. Jae, E. Mahmoud, R.F. Lobo, D.G. Vlachos, ChemCatChem 6 (2014) 508–513.
[26] J.C.V.D. Waal, P.J. Kunkeler, K. Tan, H.V. Bekkum, J. Catal. 173 (1998) 74–83.
[27] M. Balakrishnan, E.R. Sacia, A.T. Bell, Green Chem. 14 (2012) 1626.
[28] X.-L. Li, K. Zhang, S.-Y. Chen, C. Li, F. Li, H.-J. Xu, Y. Fu, Green Chem. 20 (2018) 1095–1105.
[29] X. Cao, H. Liu, J. Wei, X. Tang, X. Zeng, Y. Sun, T. Lei, G. Zhao, L. Lin, Chin. J. Catal. 40 (2019) 192–203.
[30] C.M. Piqueras, V. Puccia, D.A. Vega, M.A. Volpe, Appl. Catal. B 185 (2016) 265–271.
[31] C. Wen, Y. Cui, X. Chen, B. Zong, W.L. Dai, Appl. Catal. B 162 (2015) 483–493.
[32] L. Liu, Q. Zhao, R. Liu, L. Zhu, Appl. Catal. B 252 (2019) 198–204.
[33] W. Kang, H. Guo, A. Varma, Appl. Catal. B 249 (2019) 54–62.
[34] M.A. Dasari, P. Kiatsimkul, W.R. Sutterlin, G.J. Suppes, Appl. Catal. A 281 (2005) 225–231.
[35] H. Liu, Z. Huang, H. Kang, X. Li, C. Xia, J. Chen, H. Liu, Appl. Catal. B 220 (2018) 251–263.
[36] I.C. Freitas, R.L. Manfro, M.M.V.M. Souza, Appl. Catal. B 220 (2018) 31–41.
[37] S. Lee, H. Hsu, W. Tuan, Mater. Res.-ibero-am. J. 19 (2016) 51–56.
[38] X. Tang, J. Wei, N. Ding, Y. Sun, X. Zeng, L. Hu, S. Liu, T. Lei, L. Lin, Renewable Sustainable Energy Rev. 77 (2017) 287–296.
[39] S. Xia, R. Nie, X. Lu, L. Wang, P. Chen, Z. Hou, J. Catal. 296 (2012) 1–11.
[40] D. Verboekend, G. Vile, J. Perezramirez, Adv. Funct. Mater. 22 (2012) 916–928.
[41] S. Lopez-Orozco, A. Inayat, A. Schwab, T. Selvam, W. Schwieger, Adv. Mater. 23 (2011) 2602–2615.
[42] L. Jiang, C. Li, Z. Li, S. Zhang, Chem. Engineer. Technol. 36 (2013) 1891–1898.
[43] C. Jia, J. Gao, J. Li, F. Gu, G. Xu, Z. Zhong, F. Su, Catal. Sci. Technol. 3 (2013) 490–499.
[44] Z. Yuan, L. Wang, J. Wang, S. Xia, P. Chen, Z. Hou, X. Zheng, Appl. Catal. B 101 (2011) 431–440.
[45] D.J. Jones, J. Jiménez-Jiménez, A. Jiménez-López, P. Maireles-Torres, P. Olivera-Pastor, E. Rodriguez-Castellón, J. Rozière, Chem. Commun. 5 (1997) 431.
[46] S.J. Gentry, P.T. Walsh, J. Chem. Soc. Faraday Trans. 78 (1982) 1515–1523.
[47] C. Huo, J. Ouyang, H. Yang, Sci. Rep. 4 (2014) 3682.
[48] X.C. Shao, L.H. Duan, Y.Y. Wu, Y.C. Qin, W.G. Yu, Y. Wang, H.L. Li, Z.L. Sun, L.J. Song, Acta Phys.-Chim. Sin. 28 (2012) 1467–1473 (1467).
[49] S. Bennici, A. Gervasini, N. Ravasio, F. Zaccheria, J. Phys. Chem. B 107 (2003) 5168–5176.
[50] J.A. Bokhoven, A.M.J. Van Eerden, D.C. Van Der Koningsberger, J. Am. Chem. Soc. 125 (2003) 7435.
[51] P. Kuhn, P. Pale, J. Sommer, B. Louis, J. Phys. Chem. C 113 (2009) 2903–2910.
[52] G. Tsilomelekis, T.R. Josephson, V. Nikolakis, S. Caratzoulas, ChemSusChem 7 (2014) 117–126.
[53] R.J. van Putten, J.C. van der Waal, E. de Jong, C.B. Rasrendra, H.J. Heeres, J.G. de Vries, Chem. rev. 113 (2013) 1499–1597.
[54] Z. Hou, J. Gao, J. Guo, D. Liang, H. Lou, X. Zheng, J. Catal. 250 (2007) 331–341.